Journal of Magnetism and Magnetic Materials 475 (2019) 382–388

Contents lists available at ScienceDirect

Journal of Magnetism and Magnetic Materials

journal homepage: www.elsevier.com/locate/jmmm

Research articles

Imaging and quantification of magnetic nanoparticles: Comparison of magnetic resonance imaging and magnetic particle imaging

Hendrik Paysen*, Norbert Loewa, Karol Weber, Olaf Kosch, James Wells, Tobias Schaeffter, Frank Wiekhorst

Physikalisch-Technische Bundesanstalt, Abbestr. 2-12, 10587 Berlin, Germany

ARTICLE INFO

Keywords:
Magnetic nanoparticles
Magnetic particle imaging
Magnetic resonance imaging
Quantification
Magnetic particle spectroscopy
Nuclear magnetic resonance

ABSTRACT

Quantification and imaging of magnetic nanoparticles is of vital importance for various novel biomedical applications, like cell tracking, drug targeting or hyperthermia treatments. In this work we studied the performance of magnetic resonance imaging (MRI) and magnetic particle imaging (MPI) for quantitative imaging of magnetic nanoparticles (MNP). This was done by measurements of serial dilutions of MNP (Ferucarbotran) in two different media (water and $CuSO_4$ solution). The concentration range in which quantification was possible was determined for each technique, and the influence of the environment was analyzed and discussed. This revealed a significantly stronger influence of the surrounding medium on MRI performance as compared to MPI. All results were validated by measurements using their respective zero-dimensional (spectroscopic) techniques nuclear magnetic resonance and magnetic particle spectroscopy, showing similar behavior compared to the imaging modalities. Physical explanations of all observed effects are given, and a concentration range is determined in which the advantages of both imaging techniques can be utilized.

1. Introduction

Magnetic nanoparticles (MNP) are a prominent class of nanomaterials offering great opportunities for emerging biomedical applications [1]. The majority of these applications require, or highly benefit, from knowledge of the MNP amount and distribution in vivo. One possibility to obtain this information is to use magnetic resonance imaging (MRI). This widely used clinical imaging technique is based on measurements of a net magnetization generated by water protons in a large homogenous magnetic field, which is manipulated by gradient magnetic fields and radiofrequency pulses. This leads to the formation of a precessing transversal magnetization, which can be measured by inductive coils and used as the basis for the image reconstruction. The measured signal decays over time based on two relaxation processes: the longitudinal relaxation, characterized by the relaxation time T_1, and the transversal relaxation, characterized by the relaxation time T_2. Since these relaxation times are tissue dependent, different organs generate different signals, causing the contrast in the MR images.

The presence of MNP distorts the magnetic field in their local environment, leading to a faster dephasing of the proton spin ensemble, and hence a lower transversal relaxation time T_2 [2–4]. Therefore, MNP are visualized by a negative contrast and can be localized as “black spots” in MRI images. Quantification is also possible, since the decrease of T_2 is inversely proportional to the MNP amount. However, the use of MNP during MRI scans may also be problematic. Since the particles are visualized by negative contrast a clear separation to other sources creating field inhomogeneities, like air bubbles, can be ambiguous. Quantification based on the shift of T_2 requires knowledge of the initial relaxation time without MNP. Furthermore, the relaxation times are dependent on various parameters, which complicates the separation of the influence of the MNP alone.

A novel MNP specific imaging modality, called magnetic particle imaging (MPI), was introduced in 2005 [5]. This technique allows for the fast acquisition of 3D volumes with a temporal resolution in the milliseconds regime without using ionizing radiation. The basic concept of this technique relies on the non-linear magnetic susceptibility of MNPs. Excitation with oscillating magnetic fields superimposed by static magnetic gradient fields (for spatial encoding) leads to the formation of a response signal from the MNP, which can be measured and used for the reconstruction of the 3D MNP distribution. The signal intensity of each voxel is directly proportional to its MNP content. In MPI, signal is only generated by the MNPs which allows MNP imaging without signal contributions from the biological environment. Furthermore, possible signal changes caused by the MNP mobility can be

* Corresponding author.
E-mail address: hendrik.paysen@ptb.de (H. Paysen).

https://doi.org/10.1016/j.jmmm.2018.10.082
Received 24 June 2018; Received in revised form 16 October 2018; Accepted 16 October 2018
Available online 22 November 2018

taken into account for image reconstruction. However, no anatomical reference structures are imaged. Therefore, a second reference imaging technique, for example MRI, is typically used.

As described MRI and MPI each have their own unique advantages and disadvantages for the imaging and quantification of MNP. In this work, we investigate the quantification performance of both techniques in a simple phantom study. Of particular interest is the determination of the MNP concentration regime for complementary MRI-MPI measurements, in which the advantages of the respective method, the MNP localization and anatomical imaging of MRI and the MNP quantification of MPI, can be used.

2. Materials and methods

The quantification performance of both techniques is determined by measurements of MNP diluted in purified water at different concentrations. For this study we used Ferucarbotran (Meito Sangyo, Japan), which is the magnetically active part of the well-known MRI contrast agent Resovist (Bayer, Germany), as well as a quasi-standard reference material in MPI [6,7]. The magnetic particles consist of iron oxide crystals with sizes of about 5 nm some of which form colloidally stable clusters. The hydrodynamic diameter of the clustered particles is about 60 nm. A detailed study of all relevant magnetic properties can be found in [8,9]. Eight samples were prepared, each with a total volume of 160 µL contained within fast reaction tubes (MicroAmp, 0.2 mL Appl. Biosystems, USA) and iron concentrations ranging from 2.4 µmol/L-0.187 mol/L. The sample volume of 160 µL was chosen to have a sufficiently large MRI signal generated by water protons and to minimize air in the fast reaction tubes, which might lead to imaging artifacts in MRI.

Since the MR relaxation times of pure water are very long (T_1 and T_2 of several seconds), a second sample series with a $CuSO_4$-water solution was prepared, to simulate more realistic biological relaxation times and to demonstrate the importance of the relaxation times of the surrounding medium for MNP quantification using MRI. The $CuSO_4$ concentration was adjusted to 27 mmol/L resulting in a T_2 value between 50 and 70 ms to mimick the MRI relaxation times of liver tissue at 1.5 T [11]. A significant change of the viscosity compared to pure water is not be expected [10]. Samples containing no MNP were measured in all systems for reference.

The identical samples were measured individually using each imaging techniques. In addition to spatially resolved MRI and MPI scanners, their respective zero-dimensional (spectroscopic) methods, nuclear magnetic resonance (NMR) and magnetic particle spectroscopy (MPS) were used. Thereby the effect of the MNP on the signal generation process of the respective imaging technique can be analyzed, without the influence of the magnetic gradient systems used for spatial encoding. In the following sections each system and the measurement protocol will be shortly described.

2.1. Nuclear magnetic resonance (NMR)

The minispec mq60 NMR relaxometer (Bruker BioSpin) was used for NMR measurements of the samples (Fig. 1a). This system uses a homogenous magnetic field of 1.5 T, generated by permanent magnets. For MNP quantification, the T_2-relaxation times were determined by a Carr-Purcell-Meiboom-Gill (CPMG) spin-echo sequence [12]. This sequence uses an initial 90°-pulse for signal excitation followed by a train of 180°-pulses for signal refocusing at time intervals $n{\cdot}T_E$-$T_E/2$, n = 1,2,3…. After each 180° pulse the transversal magnetization signal was acquired at the echo times $n{\cdot}T_E$. The sampling rate, given by T_E was adjusted between T_E = 0.04 ms and TE = 3 ms to acquire most of the exponential decay. The transversal relaxation time T_2 was determined by performing a monoexponential fit to the measured data with N = 2000 points assuming that T_2 is independent on the chosen T_E.

2.2. Magnetic resonance imaging (MRI)

MRI scans were performed using the preclinical 1 T ICON system (Bruker BioSpin) with a whole-body receive coil optimized for imaging of rats (Fig. 1b). Since a minimum signal is required for the system to obtain a reliable image, the sample tubes were sealed and placed in a sample holder filled with water. A multi spin-echo CPMG sequence was used to obtain slices with a thickness of 2.5 mm of all samples. A repetition time T_R of 1.5 s and a spatial resolution of 0.625 mm over an 80 × 40 mm^2 FOV results in an acquisition time of 96 s. The minimum echo time T_E was about 5 ms for the chosen measurement parameters. 28 individual images were acquired within one scan with varying echo times. The signal intensity was averaged in a region of interest (ROI) around the sample position and an exponential fit using the image intensities were performed to determine T_2. The used echo times were adapted to acquire the full exponential signal decay. Four samples plus an additional reference sample were measured simultaneously within one imaging sequence.

2.3. Magnetic particle spectroscopy (MPS)

MPS measurements were performed with a calibrated MPS-3 system (Bruker Biospin, Fig. 1c). This system provides excitation with a homogeneous, oscillating magnetic field at 25 kHz and an amplitude adjusted to 25 mT. The magnetic response of the MNP samples is detected by gradiometric coils over time and is further analyzed in the frequency domain. Based on the non-linear magnetic susceptibility of the MNP, signal is detected for higher harmonics of the excitation frequency. For MNP quantification, the amplitudes of the third harmonic A_3 of the excitation frequency were used, which are given in units of Am^2 and are directly proportional to the quantity of particles. Each sample was measured separately for 10 s, and background signal correction was executed by subtraction of an empty scanner measurement. Due to the sample volume of 160 µL, parts of the sample exceed the homogenous sensitivity area of the receive coil, lowering the measured signal. However, this offset is the same for all measured samples and could be corrected by rescaling the data.

2.4. Magnetic particle imaging (MPI)

A preclinical 25/20 FF MPI scanner (Bruker BioSpin) was used to measure all samples (Fig. 1d). Signal excitation is done, in a similar manner to MPS, but with three orthogonal excitation fields in x/y/z-direction, with slightly different frequencies of ≈24.51/26.04/25.25 kHz and excitation amplitudes of 12 mT. Superimposing additional static magnetic field gradients of 1.25/1.25/2.5 T/m results in a (so-called) field free point (FFP) moving on a Lissajous trajectory through the field of view (FOV) volume caused by the three excitation fields. MPI signals are mainly generated by MNP in the proximity of this FFP, which are acquired by a separate receive coil to improve the sensitivity and thus the image quality [13,14]. Image reconstruction was done based on the system function approach [15,16], utilizing a measured system function acquired with a 1 µL sample Ferucarbotran at highest iron concentration (c(Fe) = 0.935 mol/L), which was measured at multiple positions all over the FOV [17]. The raw measurement signals above 80 kHz were background corrected by subtraction of empty measurements and truncated based on the signal-to-noise ratio (SNR), only keeping 40 frequency components with the highest SNR. The regularized Kaczmarz algorithm was used with a single iteration and a regularization parameter of $1{\cdot}\lambda_0 = tr(S^H S)/tr(E)$, with S being the system function and E being the identity matrix [18]. Note that identical reconstruction parameters were used for all samples for a fair comparison. The choice of these parameters massively influences the MPI image quality. Here, we focused completely on the extraction of quantitative information of the MNP amount from these data and adapted the parameters accordingly, neglecting a high spatial

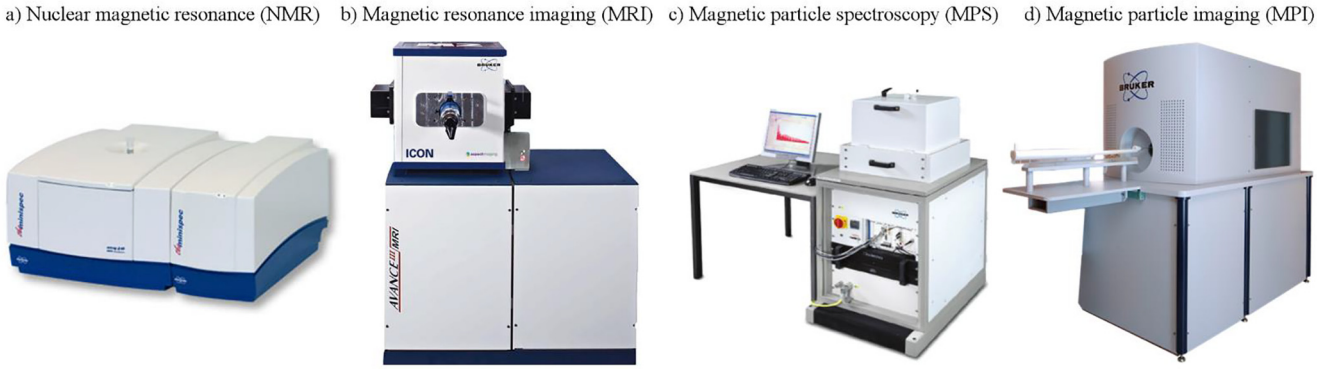

Fig. 1. Photographs of the used measurement systems: a) NMR relaxometer, Minispec mq60; b) Preclinical MRI, ICON; c) calibrated MPS device, MPS-3; d) Preclinical MPI scanner, 25/20 FF.

resolution.

The reconstruction provides 3D images of the MNP distribution over a FOV of 25 × 25 × 13 mm^3. All samples were measured individually at the center of the FOV with a total acquisition time of 10 s. The image intensities were summed up in a 3D ROI around the actual sample position for quantification.

3. Results

3.1. MNP quantification by "0D"-techniques

First, we analyze the results acquired by NMR and MPS. Fig. 2 displays the quantitative values extracted from the respective method over the iron concentration of the measured sample. In Fig. 2a), the transversal relaxation time T_2, obtained by an exponential fit based on the NMR data, is shown. The overall trend indicates an inversely linear decrease of T_2 with the iron concentration as expected. A minimal MNP concentration is required to produce a measurable signal difference compared to the T_2 value acquired without MNP. The T_2 of purified water was determined to be 2320 ms. In this case, already small iron concentrations of c(Fe) = 2.4 µmol/L led to measurable signal changes of the proton relaxation and therefore the possibility to quantify based on the changes of T_2. However, for the $CuSO_4$-water sample, T_2 without MNP was determined to be 51 ms and the first significant change based on the addition of MNP was measured at an iron concentration of 1.5 mmol/L. If the MNP concentration is below 1.5 mmol/Lthe field inhomogeneities created by the MNP are not sufficient to further decrease the overall T_2. Therefore, a minimal critical concentration is needed to measure a significant T_2 change induced by the MNP.

Since we assume that there is a concentration regime, in which the relaxation rate ${T_2}^{-1}$ (inverse of the relaxation time) scales linearly with the MNP concentration, linear fits were performed using the reciprocal data. For this purpose, only data points above the minimal concentration, needed to induce a change of T_2, were used (data selection based on visual inspection). The resulting slopes of the linear regression are listed in Table 1. Different slopes for the two different surrounding media were acquired from the NMR data with a difference of about 37%. This indicates that the magnetic properties of the MNP in the two sample types is different, which might be due to particle agglomeration. The formation of particle clusters with an overall larger diameter might influence the field inhomogeneities and therefor the transversal relaxation process of the water protons. Further details based on

Table 1
Slopes acquired by linear fits of all four measurement systems using only data above the detection limits. For MRI and NMR, the reciprocal data were used to determine the linear coefficient of the relaxation rate $R_2 = T_2^{-1}$. For the $CuSO_4$-samples no linear fit could be performed using the data acquired with MRI. For MPS and MPI the amplitude of the third harmonic excitation frequency (A_3) and the signal intensity (S) were used respectively. The values in brackets represent the mean relative deviation between the measured data, used in the fitting algorithm, and the linear fit. In general, MPS and MPI signals are normalized to the total iron amount, independent of the sample volume, in this case 160 µL. From our MPS measurements we determined values of 6.4 Am^2/kgand 5.1 Am^2/kg, for pure water and CuSO4 respectively. The MPI measurements provided values of 77.2 a. u. /kg and 61.5 a. u. /kg.

System	Parameter	Unit	Pure water	CuSO4
NMR	R_2	$\frac{ms^{-1}}{mol/L}$	141 ± 1 (22%)	89.4 ± 0.6(37%)
MPS	A_3	$\frac{\mu Am^2}{mol/L}$	57.2 ± 0.1(4%)	45.2 ± 0.2(9%)
MRI	R_2	$\frac{ms^{-1}}{mol/L}$	132 ± 1(13%)	*n. a.*
MPI	S	$\frac{a.u.}{mol/L}$	0.69 ± 0.01(3%)	0.55 ± 0.01(42%)

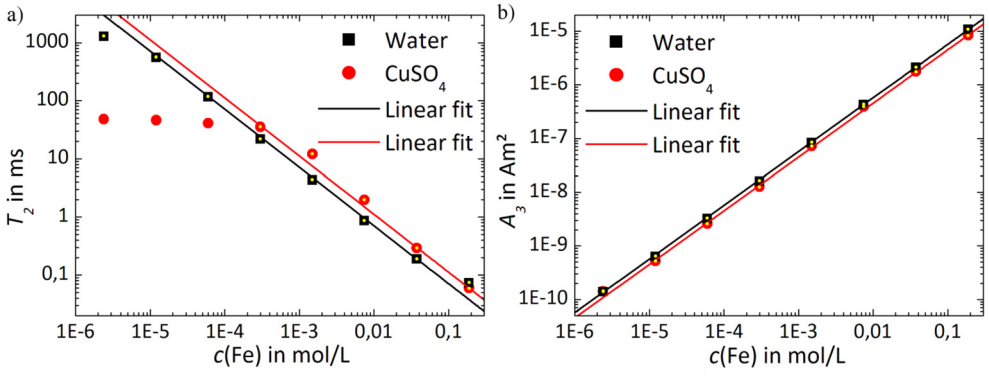

Fig. 2. Transversal relaxation time (T_2) and the amplitude of the third harmonic of the excitation frequency (A_3) acquired with NMR (a) and MPS (b) displayed over the (nominal) iron concentration c(Fe) of the measured sample. Two serial dilution of MNP were measured. The first one with MNP diluted in pure, purified water (black squares) and the second one with MNP diluted in a $CuSO_4$-water solution (red circles), to simulate more realistic tissue relaxation times. The corresponding lines denote the linear fits, which were acquired using only the data marked with a yellow dot. (For interpretation of the references to colour in this figure legend, the reader is referred to the web version of this article.)

experimental studies and simulations of the effect of particle agglomeration on the MR relaxation times can be found in [19,20]. Here, the quality of the fit was determined by calculating the mean value of the relative deviation between the data points and the linear fit (values in brackets in Table 1). From this value it can be seen, that the deviation of the $CuSO_4$ data (37%) is higher than the deviation for the water samples (22%). This might be an indication for a stronger nonlinear behavior of the MNP in the $CuSO_4$ environment. The detection limit for high iron concentrations was not reached in the measured concentration range. However, by extrapolating the linear trend, the limit of detection is expected to be about $c(\mathrm{Fe}) = 0.9\,\mathrm{mol/L}$. At this concentration, the signal decay will be too fast to detect a signal, which can be used for an exponential fit to determine T_2.

The amplitude of the third harmonic A_3 of the excitation frequency, measured with the MPS system, is depicted in Fig. 2b). In contrast to NMR, the signal intensity increases proportional to the iron concentration in the measured sample, since the signal is generated directly from the particles. The A_3 values of MNP diluted in $CuSO_4$ solution and pure water are similar for respective MNP concentration. The small deviations (largest 21%) are based on a different dynamic magnetic response of the MNP, e.g. caused by ions in the $CuSO_4$ solution which could induce the formation of MNP clusters. The influence of MNP clustering on the MPS signal is described in detail in [21,22].

MNP quantification was feasible over the whole iron concentration range of $c(\mathrm{Fe}) = 2.4\,\mu\mathrm{mol/L}$ to $c(\mathrm{Fe}) = 0.187\,\mathrm{mol/L}$. Linear fits were performed and are displayed in Fig. 2b), the slopes are listed in Table 1 showing a difference of 21% between the two media. Similar to the NMR results, the $CuSO_4$ samples show a stronger deviation (9%) compared to the linear fits than the water samples (4%), indicating nonlinear behavior. The detection limit for low iron concentrations was not reached in the measured concentration range. By extrapolating the linear behavior, the limit of detection is expected to be about $c(\mathrm{Fe}) = 0.1\,\mu\mathrm{mol/L}$ for the MPS system, since the signal is reaching the noise floor at this concentration.

3.2. MNP imaging and quantification

After analyzing the influence of MNP on the signal generation process in NMR and MPS, we next investigated whether similar behavior was observed in the respective imaging techniques. Fig. 3 displays single imaging slices acquired with MRI (a) and MPI (b) of the serial dilution of MNP in $CuSO_4$-water solution. The two MRI scans on the left show magnitude images of the diluted samples inside the water bath for the shortest echo time $T_E = 5\,\mathrm{ms}$. Imaging artifacts are visible and lead to distortions for the two highest concentrated samples one and two. Around sample three no imaging artifacts were observable, but a signal was only detected for the lowest echo time. For sample four and other samples with lower iron concentration, a signal was acquired at multiple echo times, which were averaged inside an ROI around the sample position and used for an exponential fit to determine T_2. The same procedure was performed for the measurement data of the serial dilution of MNP using pure water. The resulting T_2 values are displayed against iron concentration in Fig. 4a). Qualitatively similar behavior can be observed compared to the results acquired from NMR. T_2 decreases inversely proportional to the iron concentration, starting from a minimum “threshold”-concentration. In contrast to NMR, slightly higher T_2 values of 2424 ms (pure water) and 59 ms ($CuSO_4$-water solution) were extracted from MRI, which might be due to the lower homogeneous magnetic field strength of the MRI system. Linear fits were performed using the reciprocal data in the range, where signal changes based on the iron concentration are observed (marked by yellow dots) and the resulting slopes are presented in Table 1. No linear fit was performed for the data acquired from the $CuSO_4$-water samples, since there were too few data points above the “threshold”- concentration.

The MPI images displayed in Fig. 3b) were acquired by individual measurements of each sample. For better visualization the color bars of each image were normalized to the individual maximum reconstructed voxel amplitude. The red dots mark the nominal sample-center position inside the FOV. Note that the MPI images are blurred due to the low amounts of frequency components and the high regularization used in the image reconstruction. Therefore, the image intensity is spread over a larger volume compared to the actual sample dimensions. Sample six and all samples with a lower iron concentration, exhibit imaging artifacts, since the detected signals of the MNP at these low concentrations increasingly become distorted by the noise and background signals of the system. Around the sample positions, ROIs were defined in which the MPI signal was summed up. The resulting values are depicted over the iron concentration in Fig. 4b). Similar to the MPS results, a linear signal dependency was observed. For low iron concentrations, a constant signal, generated by noise and background signals, is acquired. The measured signals of the MNP samples diluted in the $CuSO_4$-water solution is lower compared to the signal acquired by the samples diluted in pure water. This was already observed in the MPS measurements. Linear fits were performed including all data above the noise level (marked by yellow dots) and the slopes are listed in Table 1 showing a 20% difference between both media. At low iron concentrations the MPI signal intensities show variations from the linear behavior, which are stronger compared to the MPS data. This might be because of a non-matching system function, which was acquired with a sample of MNP diluted in water. This mismatch induces additional errors in the image reconstruction process which might impair the quantification performance of MPI. Therefore, the mean relative deviation between the data points and the acquired fit is significantly higher for the $CuSO_4$ samples (42%) compared to the water samples (3%).

4. Discussion

Our results show the capability of MRI and MPI for MNP imaging and quantification. The imaging methods and their respective zero-dimensional counterparts showed similar behavior. Therefore, it can be inferred that the magnetic gradients do not significantly influence the quantification performance of the imaging systems. Based on the higher sensitivities and the usual much faster scan time of the zero-dimensional systems, they can be used for a fast characterization of different MNP tracers or different biological environments. A visual summary of the quantification results is depicted in Fig. 5. The horizontal lines represent the concentration regime, in which MRI or MPI can be used to quantify the iron concentration of the sample. The limits were determined by concentrations of the last measurable sample used in this study. It is important to note that these values are only valid when using Ferucarbotran and the chosen measurement parameters. The use of different MNP tracer types will lead to similar results but with different quantification limits. Additionally, the properties of the environment (temperature, viscosity, MNP interaction) have to be considered for MNP quantification. In this study, changes could be observed between two different surrounding media in all measurement systems. The linear fits (see Table 1) revealed differences in the slopes between 20% and 37% for the two media in all systems. A possible explanation for these differences might be attributed to agglomeration of MNP induced by the CuSO4. Additionally, the deviation of the measured data and the linear fits is greater for the CuSO4 samples compared to the water samples (see values in brackets in Table 1), which might be an indication for a stronger nonlinear behavior of the MNP. In the following, the reasons for the determined quantification limits for low and high iron concentrations with the respective imaging technique will be discussed.

MRI can quantify MNP at iron concentrations as low as $c(\mathrm{Fe}) = 2.4\,\mu\mathrm{mol/L}$ in pure water. However, for MNP in a $CuSO_4$-water solution, the lower limit is reached at much higher iron concentration $c(\mathrm{Fe}) = 0.3\,\mathrm{mmol/L}$. In MRI these lower limits are dependent on the

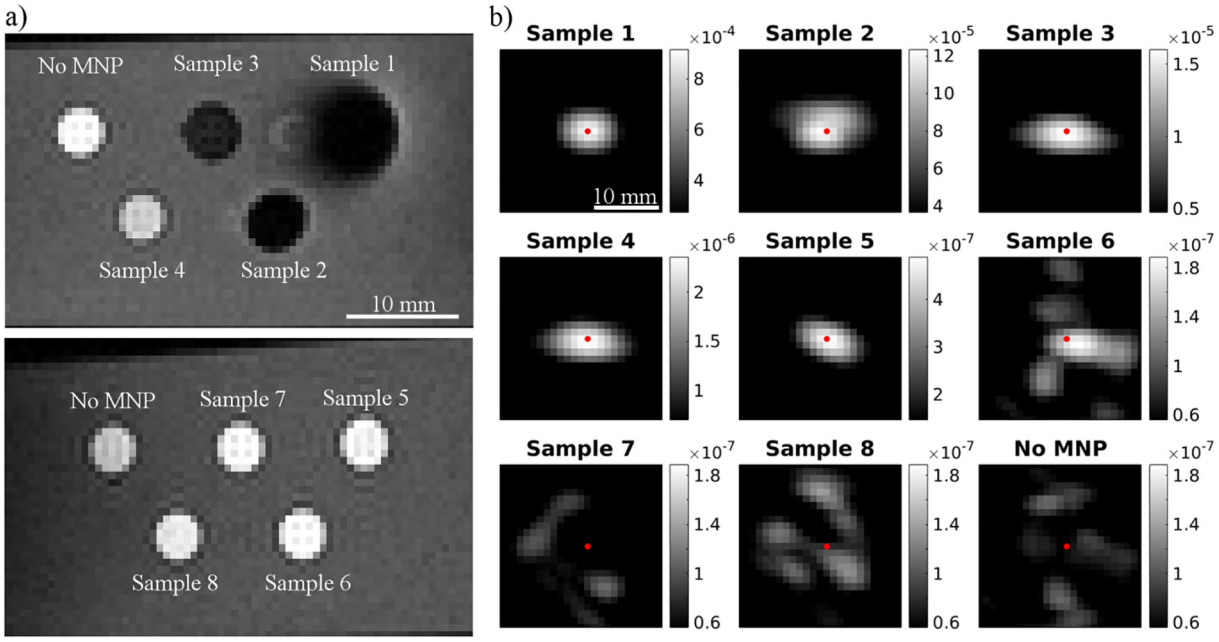

Fig. 3. Image slices acquired with MRI (a) and MPI (b) for a serial dilution of MNP in a $CuSO_4$-water solution. a) Two separate scans were performed to measure all eight samples with decreasing iron concentration (highest concentration for sample one). An additional sample tube containing no MNP was added for reference. Depicted are the image intensities acquired with the shortest $T_E = 5$ ms. Imaging artifacts can be seen in the proximity of sample one and two. The sample without MNP in the second MR scan was measured with an overall lower signal intensity based on the sample positioning and the sensitivity profile of the receive coil. b) Each sample measured individually at the center position of the FOV. The red dots mark the center of the nominal sample position. Note that the color bars (MPI signal in a.u.) were normalized individually for a better visualization. Sample six, seven and eight are distorted by imaging artifacts based on the low signal generated by the MNP at these concentrations.

initial T_2 of the medium surrounding the MNP. For pure water a large $T_2 = 2424$ ms was determined. Based on this value, already the influence of tiny iron concentrations can be detected and used for quantification based on T_2 measurements. For a lower, more realistic initial T_2 as in tissue, here $T_2 = 59$ ms adjusted by a $CuSO_4$-water solution, much higher iron concentrations are necessary to affect the transversal relaxation. Therefore, MNP quantification highly depends on the environment, and the T_2 in the region of interest should best be known before administering of MNP. This could be challenging since T_2-mapping is time-dependent and in general the relaxation times are dependent on multiple time-varying parameters such as temperature, oxygenation and diffusion rates, [23–25]. Furthermore, physiological and pathological changes can also affect T_2, making a clear identification of the contribution of MNP even harder [26,27]. The presence of MNP might also affect the longitudinal relaxation time T_1, which was neglected for all measurements presented here, since a single repetition time was used for all measurements. However, the influence of the presence on T_1, might still affect the quantification performance and will be analyzed in more detail in a future study.

The upper concentration limit for MRI quantification was determined to be $c(\mathrm{Fe}) = 1.5$ mmol/L regardless of the medium. At this concentration, the signal decay was too fast to detect with the chosen parameters, especially the chosen echo time T_E. Consequently, no exponential fit was possible, and no quantitative data were determined. Thus, imaging and localization of MNP as black spots still was possible up to an iron concentration of $c(\mathrm{Fe}) = 7.5$ mmol/L, without any major degradations in terms of image quality or spatial resolution. However, a clear separation from other possible sources for signal cancelation, like air bubbles or imaging artifacts cannot be made. For even higher concentrations, imaging artifacts distort the magnitude of MR images, making a clear localization of the MNPs difficult. In this work, we used a standard CPMG sequence with an echo time $T_E = 5$ ms. Decreasing

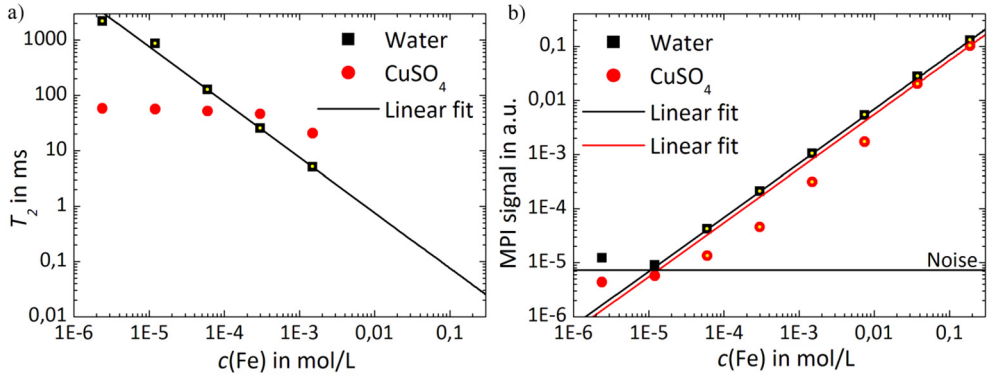

Fig. 4. Transversal relaxation time (T_2) extracted from MRI (a) and signal intensities determined by MPI (b) displayed over the iron concentration for two serial dilution of MNP in different media. For iron concentrations above 1.5 mmol/L the transversal signal decay was too fast to detect a MRI signal, therefore no relaxation time could be determined. Furthermore, a minimum iron concentration is required to detect a measurable change of T_2 depending on the surrounding media. The MPI signal intensities scale proportional to the iron concentration, above a minimum iron concentration, which generates a detectable signal above the noise floor of the system. Small changes between the surrounding media are observed based on a non-matching system function used in the image reconstruction. Linear fits were performed using only the data marked by a yellow dot. (For interpretation of the references to colour in this figure legend, the reader is referred to the web version of this article.)

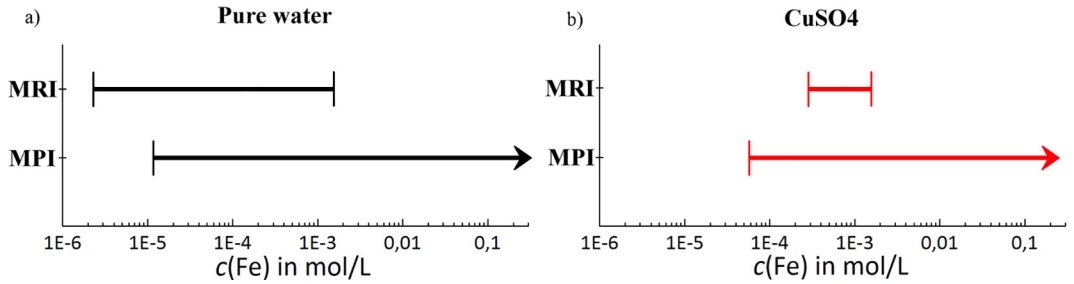

Fig. 5. Iron concentration regimes c(Fe) for MRI and MPI quantification of MNP samples (Ferucarbotran) in pure water (a) and a $CuSO_4$-water solution. For MRI, the low concentration limit is reached based on no measurable effect at the proton site induced by the MNPs. This is highly dependent on the surrounding media and their T_2. The high concentration limit is reached when the proton decay becomes too fast to be detected, which is mainly determined by the chosen (fixed) echo times T_E. In MPI, only a low iron concentration limit exists where distortions generated by random noise and background signals of the system, impede the identification of any MNP signal. The upper concentration limit is mainly limited by the hardware components of the MPI setup and was not reached in this study.

this value would allow the detection of higher iron concentrations, since a faster signal decay can be detected, then. Especially, UTE sequences ("ultrashort echo time") are capable for detection of higher iron concentrations [28–30]. However, for these methods a compromise between shorter echo times and a downgrade in spatial/temporal resolution or SNR has to be made.

In MPI a lower quantification limit of c(Fe) = 12 µmol/L in pure water was determined. The main factors influencing this limit were the noise and background signal level of the system, which hamper the signal acquisition. Further improvements for an advanced signal detection chain, would result in lower detection limits, shifting the limit to even lower concentrations. Unlike MRI, quantification limit and imaging limits are the same for MPI, since only MNP signals are acquired without any contribution from tissue. However, the image quality is affected by the iron concentration, e.g. the spatial resolution is dependent on the SNR of the raw measurement data [15,16]. By analyzing the intensities of certain frequencies components from the MPI raw data before image reconstruction, it might be possible to get quantitative information with no spatial information of the MNP locations even below the limits detection stated here [31]. The upper concentration limit of MPI is mainly determined by the saturation of certain hardware components (e.g. the low-noise amplifier), which was not reached in this study.

The influence of different media on the quantification limits of MPI is less pronounced compared to MRI, since no reference values acquired before MNP injection are necessary. The lower MPI quantification limit of c(Fe) = 60 µmol/L was determined for MNP in a $CuSO_4$-water solution. This increased value compared to the limit found in pure water is attributed to small changes of the MNP dynamic magnetization caused by the different suspension media. The presence of $CuSO_4$ might induce MNP agglomeration [21,22], changing their dynamic response. This could lower the overall response signal and additionally, change the shape of the spectrum. Therefore, the measured spectra and the previously measured spectra of the system function, which is used in the image reconstruction, might not match perfectly, inducing small errors in the reconstruction. However, if these signal changes are known, they could be corrected by adapting the system function [32,33].

5. Conclusion

In conclusion, complementary MRI-MPI measurements are possible in a certain iron concentration regime, which was determined for Ferucarbotran to be between about c(Fe) = 60 µmol/L to c(Fe) = 1.5 mmol/L. In this range, imaging and quantification of MNP can be done by MPI, while still gaining anatomical reference information from MRI with a submillimeter spatial resolution, without distortions by imaging artifacts. Therefore, the advantages of both techniques can be utilized, which might be beneficial for diagnostic purposes.

Future measurements will be performed to further analyze the influence of different biological media and different MNP tracers on the different imaging modalities.

Acknowledgment

This project was supported by the DFG research grants "AMPI: Magnetic particle imaging: Development and evaluation of novel methodology for the assessment of the aorta in vivo in a small animal model of aortic aneurysms" (grant SHA 1506/2-1) and "quantMPI: Establishment of quantitative Magnetic Particle Imaging (MPI) application oriented phantoms for preclinical investigations" (grant TR 408/9-1).

References

[1] C. Alexiou, R. Jurgons, C. Seliger, H. Iro, Medical applications of magnetic nanoparticles, J. Nanosci. Nanotechnol. 6 (2006) 2762–2768, https://doi.org/10.1166/jnn.2006.464.
[2] R.A. Brooks, F. Moiny, P. Gillis, On T2-shortening by strongly magnetized spheres: a partial refocusing model, Magn. Reson. Med. 47 (2002) 257–263, https://doi.org/10.1002/mrm.10059.
[3] Y. Gossuin, P. Gillis, A. Hocq, Q.L. Vuong, A. Roch, Magnetic resonance relaxation properties of superparamagnetic particles, Nanomed. Nanobiotechnol. 1 (2009) 299–310, https://doi.org/10.1002/wnan.036.
[4] Z.R. Stephen, F.M. Kievit, M. Zhang, Magnetite nanoparticles for medical MR imaging mater, Mater. Today 14 (2012) 330–338, https://doi.org/10.1016/S1369-7021(11)70163-8.Magnetite.
[5] B. Gleich, J. Weizenecker, Tomographic imaging using the nonlinear response of magnetic particles, Nature 435 (2005) 1214–1217, https://doi.org/10.1038/nature03808.
[6] N. Lowa, P. Knappe, F. Wiekhorst, D. Eberbeck, A.F. Thunemann, L. Trahms, How hydrodynamic fractionation influences MPI performance of resovist, IEEE Trans. Magn. 51 (2015) 1–4, https://doi.org/10.1109/TMAG.2014.2326833.
[7] J. Wells, O. Kazakova, O. Posth, U. Steinhoff, S. Petronis, L.K. Bogart, P. Southern, Q. Pankhurst, C. Johansson, Standardisation of magnetic nanoparticles in liquid suspension, J. Phys. D Appl. Phys. 50 (2017) 383003, , https://doi.org/10.1088/1361-6463/aa7fa5.
[8] R. Lawaczeck, H. Bauer, T. Frenzel, M. Hasegawa, Y. Ito, K. Kito, N. Miwa, H. Tsutsui, H. Vogler, H.J. Weinmann, Magnetic iron oxide particles coated with carboxydextran for parenteral administration and liver contrasting. Pre-clinical profile of SH U555A, Acta Radiol. 38 (1997) 584–597 http://www.ncbi.nlm.nih.gov/pubmed/9240682 (accessed September 24, 2018).
[9] D. Eberbeck, F. Wiekhorst, S. Wagner, L. Trahms, How the size distribution of magnetic nanoparticles determines their magnetic particle imaging performance, Appl. Phys. Lett. 98 (2011) 182502, , https://doi.org/10.1063/1.3586776.
[10] J. Hotlos, M. Jaskula, Densities and viscosities of CuSO4-H2SO4-H20 solutions, Hydrometallurgy 21 (1988) 1–7.
[11] Y.E. Chung, M.S. Park, M.S. Kim, E. Kim, J. Park, H.T. Song, J.Y. Choi, M.J. Kim, K.W. Kim, Quantification of superparamagnetic iron oxide-mediated signal intensity change in patients with liver cirrhosis using T2 and T2* mapping: a preliminary report, J. Magn. Reson. Imaging 31 (2010) 1379–1386, https://doi.org/10.1002/jmri.22184.
[12] S. Meiboom, D. Gill, Modified spin-echo method for measuring nuclear relaxation times, Rev. Sci. Instrum. 29 (1958) 688–691, https://doi.org/10.1063/1.1716296.
[13] H. Paysen, J. Wells, O. Kosch, U. Steinhoff, J. Franke, L. Trahms, T. Schaeffter, F. Wiekhorst, Improved sensitivity and limit-of-detection using a receive-only coil in magnetic particle imaging, Phys. Med. Biol. (2018), https://doi.org/10.1088/1361-6560/aacb87.
[14] J. Wells, H. Paysen, O. Kosch, N. Loewa, F. Schmitzberger, M. Makowski, J. Franke, L. Trahms, F. Wiekhorst, Characterizing a preclinical magnetic particle imaging

system with separate pick-up coil, IEEE Trans. Magn. (2017), https://doi.org/10.1109/TMAG.2017.2708419 1–1.
[15] J. Rahmer, J. Weizenecker, B. Gleich, J. Borgert, Signal encoding in magnetic particle imaging: properties of the system function, BMC Med. Imaging 9 (2009) 4, https://doi.org/10.1186/1471-2342-9-4.
[16] J. Rahmer, J. Weizenecker, B. Gleich, J. Borgert, Analysis of a 3-D system function measured for magnetic particle imaging, IEEE Trans. Med. Imaging 31 (2012) 1289–1299, https://doi.org/10.1109/TMI.2012.2188639.
[17] A. Weber, F. Werner, J. Weizenecker, T.M. Buzug, T. Knopp, Artifact free reconstruction with the system matrix approach by overscanning the field-free-point trajectory in magnetic particle imaging, Phys. Med. Biol. 61 (2016) 475–487, https://doi.org/10.1088/0031-9155/61/2/475.
[18] J. Weizenecker, J. Borgert, B. Gleich, A simulation study on the resolution and sensitivity of magnetic particle imaging, Phys. Med. Biol. 52 (2007) 6363–6374, https://doi.org/10.1088/0031-9155/52/21/001.
[19] A. Roch, Y. Gossuin, R.N. Muller, P. Gillis, Superparamagnetic colloid suspensions: water magnetic relaxation and clustering, J. Magn. Magn. Mater. 293 (2005) 532–539, https://doi.org/10.1016/j.jmmm.2005.01.070.
[20] Q.L. Vuong, P. Gillis, Y. Gossuin, Monte Carlo simulation and theory of proton NMR transverse relaxation induced by aggregation of magnetic particles used as MRI contrast agents, J. Magn. Reson. 212 (2011) 139–148, https://doi.org/10.1016/j.jmr.2011.06.024.
[21] E.W.C. Lim, R. Feng, Agglomeration of magnetic nanoparticles, J. Chem. Phys. 136 (2012) 124109, https://doi.org/10.1063/1.3697865.
[22] N. Löwa, M. Seidel, P. Radon, F. Wiekhorst, Magnetic nanoparticles in different biological environments analyzed by magnetic particle spectroscopy, J. Magn. Magn. Mater. 427 (2017) 133–138, https://doi.org/10.1016/j.jmmm.2016.10.096.
[23] P.A. Bottomley, T.H. Foster, R.E. Argersinger, L.M. Pfeifer, A review of normal tissue hydrogen NMR relaxation times and relaxation mechanisms from 1–100 MHz: dependence on tissue type, NMR frequency, temperature, species, excision, and age, Med. Phys. 11 (1984) 425–448, https://doi.org/10.1118/1.595535.
[24] J.M. Zhao, C.S. Clingman, M.J. Närväinen, R.A. Kauppinen, P.C.M. Van Zijl, Oxygenation and hematocrit dependence of transverse relaxation rates of blood at 3T, Magn. Reson. Med. 58 (2007) 592–597, https://doi.org/10.1002/mrm.21342.
[25] W. Oakden, G.J. Stanisz, Effects of diffusion on high-resolution quantitative T2 MRI, NMR Biomed. 27 (2014) 672–680, https://doi.org/10.1002/nbm.3104.
[26] S. Siemonsen, J. Finsterbusch, J. Matschke, A. Lorenzen, X.Q. Ding, J. Fiehler, Age-dependent normal values of T2* and T2′ in brain parenchyma, Am. J. Neuroradiol. (2008) 950–955, https://doi.org/10.3174/ajnr.A0951.
[27] T.M. Shepherd, I.I. Kirov, E. Charlson, M. Bruno, J. Babb, D.K. Sodickson, N. Ben-Eliezer, New rapid, accurate T2 quantification detects pathology in normal-appearing brain regions of relapsing-remitting MS patients, NeuroImage Clin. 14 (2017) 363–370, https://doi.org/10.1016/J.NICL.2017.01.029.
[28] W. Hong, Q. He, S. Fan, M. Carl, H. Shao, J. Chen, E.Y. Chang, J. Du, Imaging and quantification of iron-oxide nanoparticles (IONP) using MP-RAGE and UTE based sequences, Magn. Reson. Med. 78 (2017) 226–232, https://doi.org/10.1002/mrm.26371.
[29] L. Wang, X. Zhong, W. Qian, J. Huang, Z. Cao, Q. Yu, M. Lipowska, R. Lin, A. Wang, L. Yang, H. Mao, Ultrashort echo time (UTE) imaging of receptor targeted magnetic iron oxide nanoparticles in mouse tumor models, J. Magn. Reson. Imaging 40 (2014) 1071–1081, https://doi.org/10.1002/jmri.24453.
[30] C.A. Gharagouzloo, P.N. McMahon, S. Sridhar, Quantitative contrast-enhanced MRI with superparamagnetic nanoparticles using ultrashort time-to-echo pulse sequences, Magn. Reson. Med. 74 (2015) 431–441, https://doi.org/10.1002/mrm.25426.
[31] H. Paysen, J. Wells, O. Kosch, U. Steinhoff, L. Trahms, T. Schaeffter, F. Wiekhorst, Towards quantitative magnetic particle imaging: a comparison with magnetic particle spectroscopy, AIP Adv. 8 (2018) 056712, , https://doi.org/10.1063/1.5006391.
[32] T. Knopp, T.F. Sattel, S. Biederer, J. Rahmer, J. Weizenecker, B. Gleich, J. Borgert, T.M. Buzug, Model-based reconstruction for magnetic particle imaging, IEEE Trans. Med. Imaging 29 (2010) 12–18, https://doi.org/10.1109/TMI.2009.2021612.
[33] T. März, A. Weinmann, Model-based reconstruction for magnetic particle imaging in 2D and 3D, Inverse Probl. Imaging 10 (2016) 1087–1110, https://doi.org/10.3934/ipi.2016033.